A Subject-Adaptive Controller for Wrist Robotic Rehabilitation

Ali Utku Pehlivan, *Student Member, IEEE*, Fabrizio Sergi, *Member, IEEE*, and Marcia K. O'Malley, *Senior Member, IEEE*

***Abstract*—In order to derive maximum benefit from robot-assisted rehabilitation, it is critical that the implemented control algorithms promote the participant's active engagement in therapy. Assist-as-needed (AAN) controllers address this need by providing only appropriate assistance during movement execution. Often, these controllers depend on the definition of an optimal movement profile, against which the participant's movements are compared. In this paper, we present a novel subject-adaptive controller, consisting of two main components: AAN control algorithm and online trajectory recalculation. First, the AAN control algorithm is based on an adaptive controller and introduces a novel feedback gain modification algorithm. Coupled with the uniformly ultimately bounded stability property of the resulting dynamic system, the developed controller is capable of changing the amount of error allowed during movement execution, while simultaneously estimating the forces provided by the participant that contribute to movement execution. Second, we present a real-time trajectory generation algorithm based on a physiologically optimal and experimentally validated asymmetric wrist movement profile. The feedback gain modification and trajectory generation algorithms are validated with the RiceWrist system in an experimental study involving five healthy subjects, with the modified AAN adaptive controller decreasing its feedback control action when a subject shifts his behavior from passively riding along with the robot during movement to actively engaging and initiating movements to the desired on-screen targets.**

***Index Terms*—Adaptive control, exoskeletons, nonlinear systems, parallel mechanisms, robot dynamics, robotic rehabilitation.**

I. Introduction

In the United States, stroke is the leading cause of long-term disability, with approximately 795 000 individuals experiencing a stroke annually. The social and economical impacts are significant, with an estimated $38.6 billion annual cost [1]. Spinal cord injuries (SCI) also contribute to disability, with approximately 12 000 incidences in the United States each year [2]. The average age of an individual experiencing an SCI is lower than that affected by stroke, leading to total yearly direct and indirect costs of approximately $14.5 billion and $5.5 billion, respectively [3].

Manuscript received August 2, 2013; accepted June 12, 2014. Date of publication June 11, 2014; date of current version May 18, 2015. Recommended by Technical Editor E. Richer. This work was supported in part by Grants from Mission Connect, a project of the TIRR Foundation, NSF CNS-1135916, and H133P0800007-NIDRR-ARRT.

The authors are with the Mechatronics and Haptic Interfaces Laboratory, Department of Mechanical Engineering, Rice University, Houston, TX 77005 USA (e-mail: aliutku@rice.edu; fabs@rice.edu; omalleym@rice.edu).

Color versions of one or more of the figures in this paper are available online at http://ieeexplore.ieee.org.

Digital Object Identifier 10.1109/TMECH.2014.2340697

Movement rehabilitation of subjects affected by neurological lesions, including stroke and SCI, is delivered with the goal of improving function leveraging on brain and spinal cord plasticity. To achieve this objective, therapy must be intensive [4]. Robotic devices are well suited to offer multiple training sessions with consistent delivery of therapy, coupled with the opportunity to perform objective and quantitative performance evaluation of subjects throughout the course of therapy. This objective and data-driven assessment is typically not feasible with clinical tests commonly used to assess the efficacy of classical rehabilitation. Indeed, robotic devices are being increasingly included in rehabilitation protocols, and the results of clinical studies with subjects with both stroke [5] and SCI [6] support this approach.

One of the most critical areas of research in rehabilitation robotics is the development of control strategies capable of regulating physical interaction with the subject in a way that promotes plasticity and, therefore, improves motor recovery [7]. In assisting control strategies, the robotic device assists a subject to move along a desired path. As one might expect, the specific role played by the robot during therapy can significantly impact the clinical outcomes. Hogan *et al.* [8] showed that continuous passive motion-based therapy did not produce significant improvements in poststroke patients, suggesting that plasticity-mediated motor recovery requires active participation.

To ensure active participation, controllers within the assist-as-needed (AAN) paradigm [7] have been developed. Such approaches attempt to minimize the assistance provided by the robot, based on some online measurements of the subject's performance, or by defining regions of no-action, in which the robot does not assist movements. These formulations are well suited to robotic rehabilitation, given the higher intersubject variability of human movements. Additionally, such approaches are aligned with motor control studies showing that error is likely to be a driving signal for motor learning [9], [10].

Addressing some of the points above, Krebs *et al.* [11] presented an impedance control scheme based on a force-field tunnel, and a virtual wall which assists the subject by pushing them along the trajectory if the movement is slower than a predefined velocity. A fixed wait time before starting delivery of assisting forces or torques is introduced. Such an approach does not account for the fact that the subject might have heterogeneous residual motor capabilities in different regions of the workspace and might require force support only to initiate a movement, and not to complete it, or *vice versa*. A similar approach is described in [12], where an impedance controller is defined around a desired trajectory specified in the task space and regulates the

assisting forces according to the distance of the subject from the desired trajectory. The fact that the desired trajectory is only defined in the task space makes this controller independent of time, thus allowing movement velocity to be completely defined by the subject. Applying the AAN approach to a wrist rehabilitation robot, the algorithm proposed in [13] adapts the desired range of motion according to the performance of the subject, and introduces nonlinear feedback control action to minimize assistance force/torques when the error is small.

In contrast to an impedance control approach, Wolbrecht *et al.* [14] modeled the residual functional abilities of the subject and provided assistance only in the regions of the workspace in which the subject had insufficient capability. Their assistance scheme was based on an adaptive controller that used a Gaussian radial basis function (RBF) network for estimation purposes; their controller was implemented on the Pneu-WREX [15], a pneumatically actuated, 4-degree-of-freedom (DOF), serial mechanism. Inclusion of Gaussian networks in adaptive control algorithms was previously proposed for both real-time robot control [16] and for arm movement modeling purposes [17]. Additionally, to ensure continuous active participation, an adaptation law was used to decrease the assistance forces when the position error is low. A drawback of this approach is that the quality of estimate of the subjects residual capabilities is perturbed by the forgetting factor law; moreover, this approach does not allow to directly manipulate the error bounds, as is possible with force-field tunnel approaches. A required feature of adaptive controllers is a real-time trajectory recalculation. In the implementation presented in [18], the recalculated trajectory was based on a nominal minimum-jerk trajectory, executed any time the subject was ahead of the desired trajectory. Hence, the recalculated trajectory was continuous but not time-differentiable. In particular, the profile had zero velocity at the time of recalculation, implying that a new trajectory would be recalculated at the following iteration (the subject had nonzero velocity if she/he was ahead of the desired trajectory). The resulting switching action increased the computational burden and generated a discontinuous desired position profile that was likely to hinder motor recover of physiological movements.

In this study, we present a subject-adaptive controller, consisting of two novel components: the AAN control algorithm and the online trajectory recalculation. The AAN control algorithm is based on the adaptive control approach [19] and uses a Gaussian network for estimation purposes, similar to [14], and introduces a novel feedback gain modification algorithm capable of directly manipulating the error bound according to the performance of the subject. The online trajectory recalculation is based on an experimentally defined physiological wrist movement profile and generates a position trajectory that is both continuous and time differentiable.

This paper is organized as follows. Section II describes the hardware and its dynamical modeling, useful for subsequent stability analysis purposes. Section III presents the AAN controller and introduces the feedback gain modification algorithm. In Section IV, the definition of the nominal desired trajectory is made, and the online recalculation algorithm is described. The experimental results for the validation of the developed controller are presented and discussed in Section V. Finally, the conclusions of the study and remarks for future work are presented in Section VI.

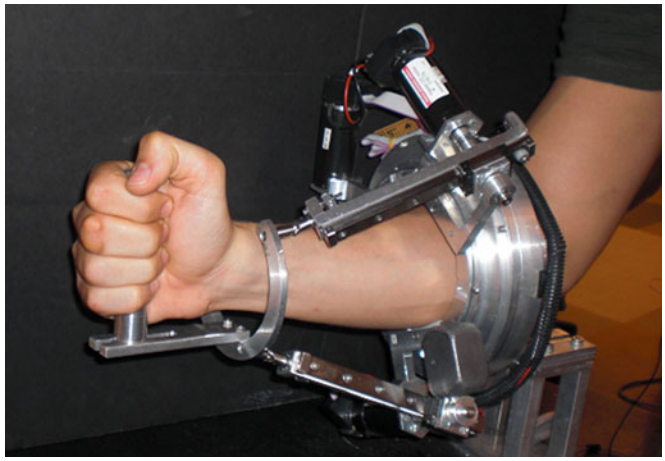

Fig. 1. RiceWrist hardware platform with a subject in neutral pose.

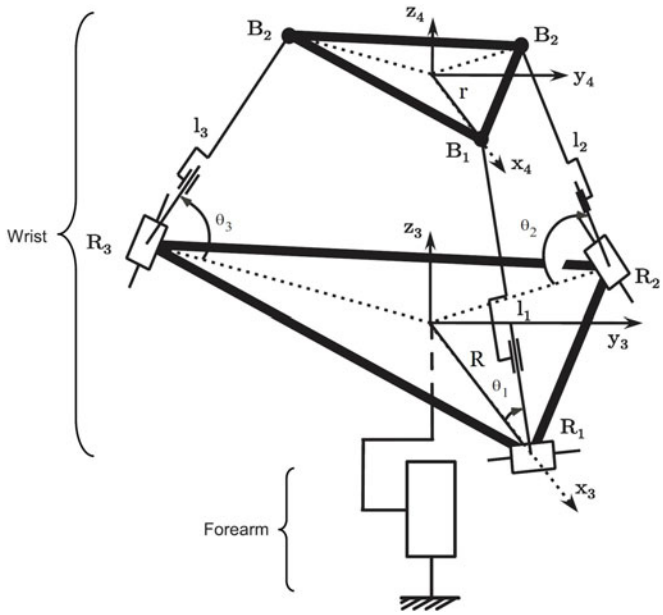

Fig. 2. Basic kinematic structure of the 4-DOF serial-in-parallel RiceWrist which employs a 3-RPS parallel mechanism at the wrist module and a revolute joint at the forearm. Reference frames 3 and 4 are attached to the base plate and end effector of the 3-RPS mechanism, respectively. Rotation around x_4 with respect to reference frame 3 corresponds to wrist FE, and rotation around y_4 with respect to reference frame 3 corresponds to wrist RUD.

II. Hardware Description and Modeling

The RiceWrist [20] is a wrist and forearm exoskeletal robotic device (see Fig. 1). The basic kinematic structure of the 4-DOF serial-in-parallel mechanism is depicted in Fig. 2. The exoskeleton is comprised of a 3-revolute-prismatic-spherical (RPS) wrist, to support wrist flexion/extension (FE) and radial/ulnar deviation (RUD), and a revolute joint for forearm pronation/supination (PS). The final DOF of the platform is

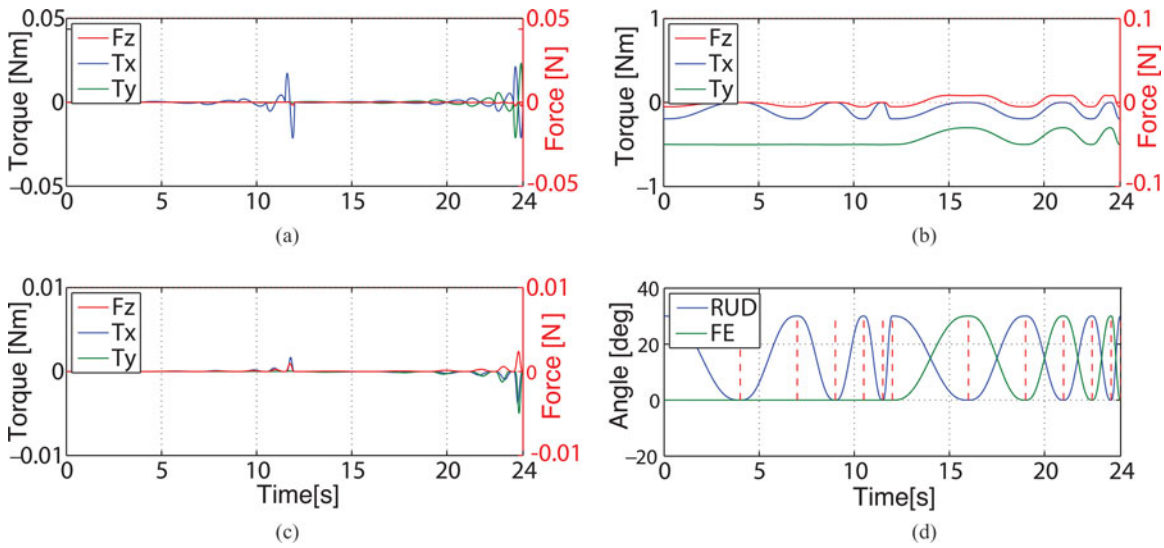

Fig. 3. Inverse dynamics simulation of the parallel portion of the RiceWrist for combination of FE and RUD movements. The desired angles are calculated as typical wrist motion profiles, with velocity profile determined by a symmetric beta function, with 30° movement extent and variable reaching time, from 4 to 0.5 s. Instants of target reaching are represented by red dashed lines in (d), and the corresponding torques are calculated in the domain of output coordinates, including (a) inertial force–torques, (b) gravitational force–torques, and (c) Coriolis/centrifugal force–torques.

translation (distance of bottom plate from top plate) and accounts for minor misalignments of the wrist rotation axes with the device. The dynamic equations of the system can be represented in the form

$$M(x)\ddot{x} + C(x,\dot{x})\dot{x} + g(x) = F_r + F_p \tag{1}$$

where x is a 4×1 vector of end-effector position (*independent coordinates*), M is the 4×4 inertia matrix, C is the 4×4 matrix which represents Coriolis/centrifugal terms, G is the 4×1 gravity vector, F_r is the 4×1 vector of forces applied by the actuators, and F_p is the 4×1 vector of forces applied by subject at the end effector (handle) which is mapped to the joint space by the transpose of the inverse of the Jacobian of the mechanism.

Using the formulation in [21], it can be shown that the dynamical equations of the RiceWrist can be expressed in the form of (1) and possess identical properties as open-chain serial mechanisms. The important distinction, however, is that the obtained dynamical model is valid only locally, i.e., the domain of the generalized coordinates (x) is a bounded and closed set (Ω) rather than the whole n-dimensional real space (n corresponds to the number of DOF of the device, in our case $n = 4$) [21]

$$x \in \Omega, \quad \text{where} \quad \Omega \subset \Re^n$$

In our previous work [22], we determined that a conservative estimate of the domain of validity of the reduced kinematic model of the parallel portion of the RiceWrist is well within the requirements for wrist movement-based rehabilitation therapy. In particular, we determined that the reduced model is valid within very large margins, for both FE and RUD movements with velocities on the order of 30–100 °/s.

We developed an accurate dynamical model of the parallel portion of the RiceWrist, following the formulation presented in [21], that is valid in this reduced domain. Such an approach allows obtaining an estimate of inertial and Coriolis torques required to produce movement profiles such as those required for wrist rehabilitation therapy, through inverse-dynamics simulations, that will be useful for subsequent stability analysis of the proposed adaptive controller (see Appendix for details).

The results of the inverse dynamics simulation are shown in Fig. 3. It can be seen that for physiological wrist pointing profiles (30° angle extent, minimum reach time of 0.5 s), inertial and Coriolis components of force/torques are negligible compared to the gravitational torques, and are in general lower than 0.05 N · m, which is around 2% of the maximum torque delivered by the RiceWrist during continuous therapy. This simulation provides a quantitative foundation that enables the quasi-static approximation that will be used in the adaptive control method, described in the following section.

III. AAN Controller

In this section, we introduce the AAN controller which employs an adaptive control algorithm developed by Slotine and Li [19], and a feedback gain modification algorithm, which modifies the amount of permissible error according to the performance of the subject. First, we describe the adaptive controller and conduct the stability analysis in order to show the uniformly ultimate boundedness of the errors. Then, we build the development of the feedback gain modification algorithm on the results of previous description and analysis.

A. Adaptive Controller

In our formulation, we develop the controller in task space, because we wish to abide by the formulation in [18], which confers a clear physical meaning to the regressor matrix, where the construction of the regressor matrix is an integral step in the formulation of the controller.

Having represented the dynamic equations of the system in the form of (1), we define the tracking error as $\tilde{x}(t) = x(t) - x_d(t)$, where $x_d(t)$ is the desired end effector trajectory which is at least twice differentiable. Furthermore, let us define the sliding-mode variables

$$\begin{aligned} r &= \dot{\tilde{x}} + \Lambda\tilde{x} = (\dot{x} - \dot{x_d}) + \Lambda(x - x_d) \\ v &= \dot{x_d} - \Lambda\tilde{x} = \dot{x_d} - \Lambda(x - x_d) \\ a &= \dot{v} \end{aligned} \tag{2}$$

where Λ is a 4×4 constant, positive-definite, symmetric matrix.

Since the system dynamics are linear in terms of system parameters, they can be represented as a multiplication of a regressor matrix, which includes the known functions of the system equations, and an unknown vector. We now assume that the forces applied by the subject F_p depend primarily on the orientation of the hand. Hence, the force field F_p is dependent on the three rotational elements of x, $x_{\rm rot}$, defining the posture of the wrist joint. We further assume that F_p is linearly parameterizable.

In our formulation, different from what Slotine and Li proposed in [19], we use a control law that only estimates the position-dependent elements ($G(x)$ and F_p) and does not account for the inertial and Coriolis/centrifugal terms $M(x)\ddot{x}$ and $C(x, \dot{x})\dot{x}$. Through our modification, we relax the requirement of asymptotic stability in favor of uniformly ultimately bounded stability (see Section III-A for stability analysis), thereby enabling direct modulation of the system error bounds.

Consider the following control law:

$$F_r = \hat{G}(x) - \hat{F}_p - K_D r \tag{3}$$

where $\hat{G}$ is the estimate of the gravitational term, $\hat{F}_p$ is the estimate of the forces coming from the subject, and K_D is a symmetric positive-definite feedback gain matrix.

As stated above, both $G(x)$ and F_p are linearly parameterizable, and they can be modeled as

$$Y\hat{\theta} = \hat{G}(x) - \hat{F}_p \tag{4}$$

where Y is a $4 \times m$ regressor matrix which contains known functions of state x, and $\hat{\theta}$ is the $m \times 1$ vector containing estimates of unknown system parameters. We used Gaussian RBFs to model both $G(x)$ and F_p. The rationale to use Gaussian RBFs is that any continuous function, not necessarily infinitely smooth, can be uniformly approximated by linear combinations of Gaussian RBFs [23]. We partitioned each rotational DOF of the robot in four equally spaced intervals, yielding five nodes for every rotational DOF (located at -20°, -10°, 0°, 10°, 20°) and a total number of 125 points in the 3-D space defined by the RiceWrist rotational DOFs. We then defined 125 RBFs throughout the workspace of the RiceWrist as

$$g_n = \exp(-\|x_{\rm rot} - \mu_n\|^2 / 2\sigma^2) \tag{5}$$

where g_n is the nth Gaussian RBF, $x_{\rm rot}$ is the 3×1 current orientation of the RiceWrist's end-effector, μ_n is the 3×1 location of the nth Gaussian RBF, and σ is a constant which defines the width of the function. By keeping the number of functions as low as possible, we aimed to decrease the expense of computation and to avoid estimation of unrealistically irregular force fields [24]. The forces coming from the subject are parameterized using these 125 RBFs. The vector of Gaussian RBFs is defined as

$$g = [g_1 \; g_2 \; ... \; g_{125}]^T. \tag{6}$$

Consequently, the regressor matrix is defined as

$$Y^{4\times 500} = \begin{bmatrix} g^T & 0 & 0 & 0 \\ 0 & g^T & 0 & 0 \\ 0 & 0 & g^T & 0 \\ 0 & 0 & 0 & g^T \end{bmatrix}. \tag{7}$$

In order to develop the adaptation law through stability analysis of the controller, we first choose the Lyapunov function candidate as

$$V(t) = \frac{1}{2}[r^T M r + \tilde{\theta}^T \Gamma \tilde{\theta}] \tag{8}$$

where Γ is a 4×4 constant, positive-definite, symmetric matrix, and $\tilde{\theta}(t) = \hat{\theta} - \theta$. Next, we differentiate (8) and use the following relations beside the skew-symmetry property:

$$\begin{aligned} \ddot{x} &= \dot{r} + a \\ \dot{x} &= r + v \\ Y\hat{\theta} &= \hat{G}(x) - \hat{F}_p \end{aligned}$$

in order to obtain following equation:

$$\dot{V}(t) = -r^T K_D r + r^T Y\tilde{\theta} + \tilde{\theta}^T \Gamma \dot{\tilde{\theta}} + B \tag{9}$$

where

$$B = -r^T C v - r^T M a. \tag{10}$$

We use the adaptation law suggested in [19]

$$\dot{\tilde{\theta}} = -\Gamma^{-1} Y^T r. \tag{11}$$

The adaptation law, when substituted into (9), produces

$$\dot{V}(t) = -r^T K_D r + B. \tag{12}$$

Hence, we show that the controller is uniformly ultimately bounded, i.e., the error always stays within a certain bound, due to the existence of B. The condition

$$|r^T K_D r| > |B| \tag{13}$$

has to be verified, for the derivative of V to be negative. Two important points are worthy of note. First, the term B is fairly small for rehabilitation applications with low velocity and acceleration values, as shown in Section II. Second, from (12), it is visible that the error bound can be modulated by the K_D term. In fact, the feedback gain modification algorithm, described in the following section, exploits the uniform ultimate boundedness of the controller and modifies the error bound by modulating the K_D term.

Note that the feedback part of the controller (3) is in essence a PD controller, while the feedforward part of the controller is the estimate of the forces coming from the subject. In case of a drastic change in the subject's force input, the controller is still providing assistance according to the previously determined estimate. In this situation, the dynamical system is equivalent to

a PD controller with disturbance. The disturbance includes the wrong feedforward estimate and the instantaneous input from the subject. Hence, considering a possibility of a drastic change in the subject's force input, we implemented a software stop which is based on a threshold error (15°) between the desired and actual positions, immediately inactivating the amplifiers when this condition is met.

B. Feedback Gain Modification Algorithm

Although the adaptive controller described in Section III-A considers the input from the subject and adjusts the robot torque input accordingly, the subjects might still let the robot take control. To address this issue, Wolbrecht *et al.* [14] propose a forgetting factor algorithm which decays learned parameter estimates when error is low. We follow a different approach to AAN control, that aims at introducing error in the execution of movements during rehabilitation, through the modulation of the controller feedback gain. This is motivated by motor control studies showing that error is likely to be a driving signal for motor learning [9], [10]. Through the uniform ultimate boundedness of our formulation, the feedback gain modification directly manipulates the admissible error bounds and the amount of force support. Hence, instead of requiring the errors to become zero, our approach tolerates error and manipulates the error bound according to the performance of the subject. Furthermore, the proposed approach does not apply any modification to the adaptation law of the controller [19]; hence, it does not interfere with the quality of force estimation.

The algorithm is based on the definition of a minimum and a maximum feedback gain (diagonal matrices $K_{D_{\rm MAX}}$, $K_{D_{\rm MIN}}$), which are determined experimentally according to predetermined bounds for average errors ($r_{\rm MIN}$, $r_{\rm MAX}$). This is done by considering (12) and modifying the gain along the desired movement trajectory according to the subject's performance. The feedback gain is updated in a discrete manner, at the end of every single-movement task. The following difference equation was used to update the scalar feedback gain $k_{D_{i,j}}$, for the task i, for the jth DOF:

$$k_{D_{i,j}} = (1 - 1/\tau)k_{D_{i-1,j}} + A/\tau \tag{14}$$

where τ is an update constant (units of task numbers), and A is the convergence value of the first-order difference equation, which is modified according to the relation

$$A = \begin{cases} k_{D_{\rm MIN},j}, & \text{if} \quad \alpha < 0 \\ (1-\alpha_j)k_{D_{\rm MIN},j} + \alpha_j k_{D_{\rm MAX},j}, & \text{if} \quad 0 \le \alpha \le 1 \\ k_{D_{\rm MAX},j}, & \text{if} \quad \alpha > 1 \end{cases} \tag{15}$$

where α_j is defined with the linear relation

$$\alpha_j = \frac{r_{av,j} - r_{\min,j}}{r_{\max,j} - r_{\min,j}} \tag{16}$$

where $r_{\rm av,j}$ is the average error of the subject in DOF j during a single movement task.

IV. Definition of a Desired Trajectory

Wrist movements have relevant dynamical differences compared to shoulder and elbow movements [25], [26]. It is thus reasonable to expect that kinematic synergies observed for planar shoulder and elbow movements might not be fully replicated in wrist movements. In particular, a recent study [27] measured velocity profiles of wrist pointing movements involving wrist FE and RUD, using nonlinear least-square fitting as a benchmark to compare different analytic forms of velocity profiles. A major finding of that study was the tendency of asymmetric profiles to provide improved goodness-of-fit results, compared to profiles with inherent symmetry, such as the minimum jerk profile. Some methodological limitations (i.e., nonunicity of the fit, dependence of the solution on the initial parameters given for the fit, tendency of estimates to converge to velocity profiles with nonzero initial and final velocities) and the inherent variability observed in wrist pointing movements prevent drawing strong conclusions, such as the definition of a nominal physiological velocity profile. However, the observed asymmetry in velocity profiles seems to be a common trait of wrist pointing motion that needs to be considered when defining a desired trajectory for robot-aided rehabilitation applications.

A. Experimental Study With Healthy Subjects

In order to define a physiological representation of the desired wrist movement profile during pointing movements, to be employed for the adaptive control scheme presented in this paper, we conducted an experimental study with healthy subjects.

1) Protocol: The experiment involved seven healthy male individuals, ages 23–29 years, who were asked to perform movements in FE or RUD using the RiceWrist. During the experiment, the RiceWrist was powered OFF and used only in registration mode, minimally perturbing subjects' movements due to its intrinsic backdriveability.[1] A graphical display was provided to visually guide subjects during the execution of a point-to-point movement. Two experiments were performed with each subject, allowing separate analysis of wrist FE and RUD movements. For either movement, two target locations were used, corresponding to a displacement away from the center of the display either to the right or left (FE), or up and down (RUD). The center of the display corresponded to the neutral wrist position. A target would change color from black to blue to suggest a movement toward that target. For the first 0.75 s, the target would remain blue, eventually turning to red, to indicate that a pointing movement toward that target should last for 0.75 s. The target remained red for 0.75 s, before turning black as the next target changed color to blue. Eighty targets per DOF were presented in a random order; after every peripheral target, the next movement was always imposed to be toward the central target. Movement extent was set to 25°. Subjects were allowed to practice freely with the device until they felt comfortable with the device and the visual display, and after this practice session, data collection began.

[1]Torques required to back drive the RiceWrist are on the same order of those of the device used in [27]

2) Data Analysis: Due to the inherent unidimensionality of the task (the maximum straight line deviation of successful movements was lower than 0.5°), velocity profiles were calculated as time derivatives of the measured Euler angles, using the X-Y-Z sequence in moving frame. Encoder data were acquired continuously at 1000 Hz; velocity profiles were extracted in postprocessing using a Savitzky-Golay filter, performing a local fourth-order polynomial fit, in a moving window of amplitude 200 ms. Having calculated the instant $t_{\max}$ with maximum instantaneous velocity $v_{\max}$, segmentation of reaching movements was performed by defining the times t_{in} and t_{end} of movement start and end, respectively, by searching the minimum and maximum times in which the condition $|v(t^*)| > 0.05 \cdot |v(t_{\max})|$ was verified in a continuous range comprising the time $t_{\max}$. Segmented movement profiles were then visually inspected in order to ensure evaluation of movement profiles containing a single peak, following the same procedure reported in [27]. One hundred and four out of 638 tasks (16%) were discarded for FE, and 187 out of 622 tasks (30%) were discarded for RUD movements. To account for different movement durations, computed times (hereafter referred as t') were mapped into a normalized temporal [0,1] range.

Two indices of symmetry of the acquired velocity profiles were considered. The first index was *peak location*, defined $t_{\text{peak}} = t'_{\max}$. The second index was *skewness*, defined for a probability distribution function as $skewness = E[(\frac{(X-\mu)}{\sigma})^3]$. In order to compute $skewness$, the velocity profile was normalized to have unitary area and *skewness* computed numerically from the acquired velocity profile, assuming the latter as the probability distribution.

The calculated symmetry indices were subject to statistical inference tests. A Jarque–Bera test [28] was applied in order to test the null hypothesis so that the samples come from a normal distribution with unknown mean and variance. Due to nonnormality of the measured indices, two nonparametric tests were then applied: the Wilcoxon signed-rank [29] and the sign test [30], in order to test whether both indices of symmetry come from a distribution with a median corresponding to that of a symmetric profile.

3) Results: Symmetry indices for the 969 completed tasks are reported in Fig. 4. The mean value of the measured $skewness$ equals -0.041 (standard deviation: 0.185), while the mean value of peak location index t_{peak} equals 0.52 (standard deviation: 0.078). Both indices suggest the prevalence of asymmetric profiles with a negative skewed distribution. The Jarque–Bera test was applied to test the normality of distribution of both symmetry indices, showing a very high-statistical significance for the rejection of the hypothesis that the symmetry indices are normally distributed ($p < 0.001$ in both cases). A Wilcoxon signed-rank test was then used to test the null hypothesis that the measured indices of symmetry come from a distribution with a median corresponding to that of a symmetric profile ($skewness = 0$ and $t_{\text{peak}} = 0.5$). Both tests rejected the null hypothesis with strong statistical significance ($p < 0.001$) in both cases, giving the following ranges for the median of computed indices of symmetry, at the $p < 0.05$ confidence level: $skewness = -0.05 \pm 0.01$, $t_{\text{peak}} = 0.528 \pm 0.005$.

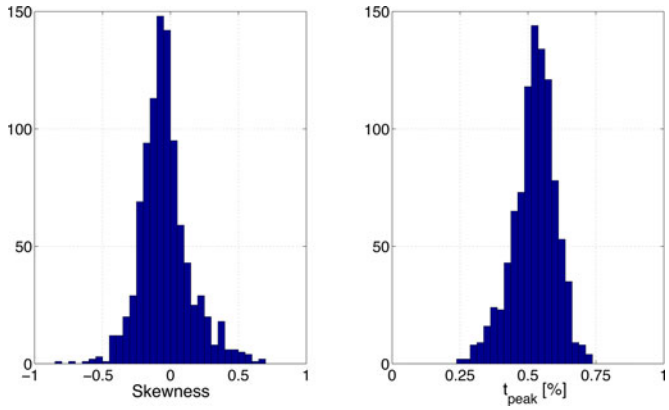

Fig. 4. Histograms of the extracted indices of symmetry, obtained combining results from the FE and RUD experiments. Skewness distribution mean is -0.041, standard deviation equals 0.185, while peak percentage mean is 0.52, with standard deviation 0.078

Ultimately, due to the asymmetric distributions of both indices of symmetry considered, the sign test was eventually used, rejecting the hypothesis of symmetric movement profiles ($p < 0.001$ in both cases), and giving the following estimate of medians, at the $p < 0.05$ confidence level: $skewness = -0.06 \pm 0.012$, $t_{\text{peak}} = 0.53 \pm 0.005$, thus giving evidence for the asymmetry of single peak wrist pointing profiles.

B. Definition of a Nominal Trajectory for Wrist Pointing Movements

Despite the abundance of proposed analytical representation of wrist pointing movement velocity profiles [31], successful integration in a robot control scheme introduces several requirements, such as continuity and ease of computation, that were not necessarily considered in previous studies. As a working hypothesis to demonstrate our control approach, we defined the desired movement profile using the beta function as

$$v(t) = P_1(t - P_2)^{P_3}(P_4 - t)^{P_5}, \quad P_2 \le t \le P_4. \tag{17}$$

As proposed in [32], the beta function is a convenient function that can be used to accurately describe and synthesize both human and robot movements: it can represent either symmetric or asymmetric movement profiles, and its parameters can be tuned very easily in a decoupled fashion. P_2 indeed corresponds to the time of movement start, P_4 represents the time of movement end, P_1 is a scaling factor that can be used to represent movements of different extents, and finally, P_3 and P_5 can be modified in order to obtain a given degree of (a)symmetry. In particular, the location of the single peak in the velocity profile can be calculated as

$$t_{\text{peak},\beta} = \frac{P_3P_4 + P_2P_5}{P_3 + P_5} \tag{18}$$

while the profile skewness can be calculated as

$$skewness_\beta = 2\frac{(P_5 - P_3)\sqrt{P_3 + P_5 + 3}}{(P_3 + P_5 + 4)\sqrt{(P_3 + 1)(P_5 + 1)}}. \tag{19}$$

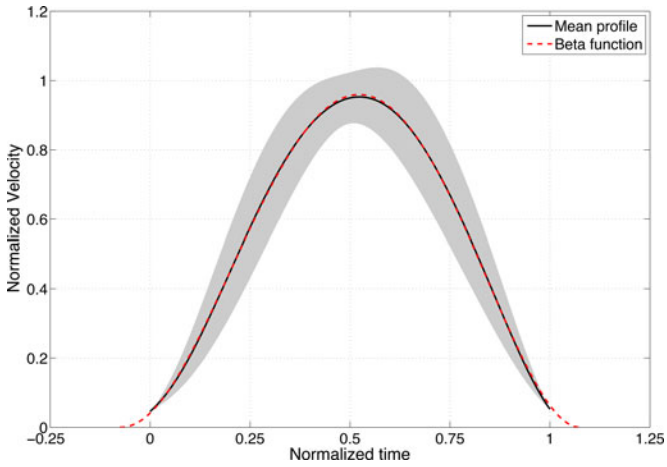

Fig. 5. Results of least-square fitting between the mean profile obtained from the 969 successful trials, normalized in amplitude and time, and a beta function profile defined by (17), with error bounds representing one standard deviation above and below the mean value. $R^2 = 0.9998$.

Finally, parameter P_1 accounts for movements of different extent, considering the following relation:

$$\int_{P_2}^{P_4} v(\tau)\mathrm{d}\tau = P_1 \frac{(-P_2+P_4)^{1+P_3+P_5}\Gamma(1+P_3)\Gamma(1+P_5)}{\Gamma(2+P_3+P_5)} \tag{20}$$

where $\Gamma(\cdot)$ is the gamma function. Equations (18)–(20), in combination with the initial and final value conditions

$$v(t=P_2) = v(t=P_4) = 0, \quad P_2 < P_4 \tag{21}$$

show that a generic, asymmetric, single-peaked movement profile of any duration t_d can be represented as (17), by setting parameter $P_2 = 0$, parameter $P_4 = t_d$, parameters P_3 and P_5 to verify some conditions on profile symmetry, and finally, modulating parameter P_1 in order to generate smooth movements of different extent (20).

The proposed approach allows the definition of a smooth and natural desired trajectory for wrist movements in free space. Fig. 5 shows that the beta function can be successfully used to represent wrist movements during pointing tasks. Least-square fitting has been applied to the mean profile extracted during the experiments reported above (velocity profiles in the normalized time domain were normalized in amplitude), and a goodness-of-fit coefficient $R^2 = 0.9998$ was found.

C. Online Recalculation of the Desired Trajectory

Special care was taken to avoid the application of forces resisting directed movements toward the target, in the case in which the subject is actually "performing better," compared to the previously defined "nominal" movement. For this reason, an explicit real-time trajectory recalculation routine was implemented, which guarantees the recalculation of trajectories respecting the asymmetry observed in healthy individuals during wrist pointing movements and generates a position profile that is both continuous and time-differentiable. In order to increase speed of computation with consequent possibility of real-time implementation, the online recalculation of desired trajectory was determined through piecewise polynomial functions, whose parameters can be calculated using algorithms requiring the solution of a set of linear equations.

Defining $y_p(t)$ the position of the subject measured by the device, and $y_{\mathrm{nom}}(t)$ the nominal desired trajectory with target position y_t, we define t_1 as the time of trajectory recalculation, i.e.,

$$t_1 \colon |y_p(t_1) - y_t| < |y_{\mathrm{nom}}(t_1) - y_t|. \tag{22}$$

If t_1 exists, the trajectory $y_{\mathrm{nom}}(t)$ is substituted by a new desired trajectory $y_{\mathrm{recalc}}(t)$. The goal of trajectory recalculation is to provide a continuous and differentiable function, with zero final velocity and acceleration, with possibility to control both the location of the velocity profile peak (occurring at $t = t_2$) and of movement duration, to provide continuous levels of challenge to the user.

In the implemented trajectory recalculation scheme, we distinguish between two cases. In the first case, $t_1 < t_2$, and the desired trajectory is constructed as a piecewise continuous function, defined as two fourth-order polynomials S_1 and S_2, defined in the intervals $[t_1, t_2]$ and $[t_2, t_3]$, as follows:

$$y_{\mathrm{recalc}}(t) = \begin{cases} S_1(t-t_1), & \text{if } t \in [t_1, t_2] \\ S_2(t-t_2), & \text{if } t \in [t_2, t_3]. \end{cases} \tag{23}$$

The ten constants defining polynomials $S_1(t)$ and $S_2(t)$ are defined by solving a linear system deriving from the following ten constraint equations:

$$\begin{aligned} &S_1(t_1) = y_p(t_1), \quad S_1'(t_1) = \dot{y}_p(t_1), \quad S_1''(t_2) = S_2''(t_2) = 0 \\ &S_2(t_3) = y_t, \quad S_1'''(t_2) = S_2'''(t_2), \quad S_1'(t_2) = S_2'(t_2) \\ &S_1(t_2) = S_2(t_2), \quad S_2'(t_3) = 0, \quad S_2''(t_3) = 0. \end{aligned}$$

The imposed conditions guarantee class C^3 of the function in the interval $[t_1, t_2]$, zero final (i.e., $t = t_3$) velocity and acceleration, continuity of the desired position profile with $y_p(t)$ measured before recalculation, and generate a velocity profile with a peak at the desired time t_2. In the second case, $t_1 > t_2$, and a third-order polynomial profile $S_3(t)$ is defined through interpolation between the recalculation point t_1 and the final point t_3. The described algorithm can be implemented in real time in a computationally efficient way since it requires solution of a linear system of equations, with a maximum order of ten (the order drops to four for the simpler interpolation case $t_1 > t_2$).

A simulation experiment (see Fig. 6) shows the performance of the trajectory recalculation algorithm for $t_3 = 0.95$ (5% reduction of allocated time), and $t_{\mathrm{peak}} = 0.52$ (moderate profile asymmetry). The required continuity of the profiles in both position and velocity is achieved.

Real-time implementation also allows for modulation of parameter t_3 (total allocated time), which can be modified at every recalculation as

$$t_3(k,i) = t_3(k-1,i) - S(k)T \tag{24}$$

where S is a binary flag, whose value of one at iteration k indicates recalculation at that iteration, and T defines the decrease

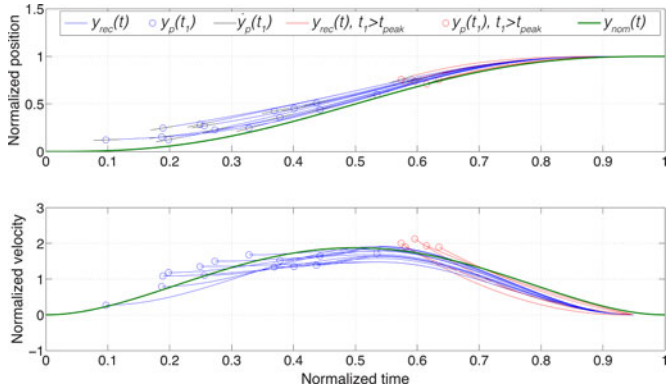

Fig. 6. Trajectory recalculation for random values of t_1 and $y_p(t_1)$, (top) position profile, (bottom) velocity profile. Initial conditions are represented by circles, with initial derivatives $\dot{y}_p(t_1)$ symbolized by black lines crossing the circle, around it. Profiles recalculated through piecewise polynomial interpolation ($t_1 < t_{\rm peak}$) are reported in blue, while those recalculated through simple polynomial interpolation ($t_1 \geq t_{\rm peak}$) are reported in red. The green lines report the nominal position and velocity profiles $y_{\rm nom}$, with target time $t_3 = 1$. Recalculated profiles have a reduced target reaching time $t_3 = 0.95$, compared to the nominal profile, and have the velocity peak at $t_{\rm peak} = 0.52$.

in t_3 introduced by one occurrence of a recalculation. For every target reaching task i, the initial allocated time $t_3(1,i)$ can be set evaluating a binary flag $R(i)$ that is true when trajectory recalculation occurs during target reaching task i, and multiplying by a constant $\Delta > 1$ that increases allocated time as

$$t_3(1,i) = \begin{cases} t_3(\text{end}, i-1), & \text{if } R(i-1) = 1 \\ \Delta t_3(\text{end}, i-1), & \text{if } R(i-1) = 0 \end{cases} \tag{25}$$

After a successful movement, the resulting value of t_3 is passed for the generation of the new desired trajectory of the following target by imposing $P_4 = t_3$ and calculating the other constants using (18–20).

The recalculation steps described above were integrated in the real-time controller as follows. Before each movement starts, a desired profile is constructed as the integral of the beta function velocity profile, with t_3 determined as in (25), and with a specified initial time $t_3(1,1)$. The system continuously measures the position of the handle; when recalculation occurs (i.e., condition (22) is verified), the desired trajectory is computed as a piecewise polynomial function, using (23), and parameter t_3 is updated as in (24), until the current movement is completed and the updated value of parameter t_3 is passed for the next task using (25).

V. Experimental Validation

Experiments have been conducted to validate the developed controller, taking into special account the novel features introduced in the current implementation: the feedback gain modification algorithm for the adaptive controller and the trajectory recalculation. Additionally, demonstration of the simultaneous implementation of the two modules is presented and a detailed analysis of the controller performance is provided. The controller was implemented in Simulink (The MathWorks, Inc.), software translated into real-time code using QuaRC (Quanser Inc.) and executed at a sampling rate of 1kHz. All experimental results are presented for isolated movements of one of the DOFs of the robot, FE of the wrist, since we anticipate rehabilitation protocols to target individual DOFs of the RiceWrist, rather than coordinated movements, since studies suggest that repetitive isolated movements have positive effect on the results of the motor rehabilitation of subjects with stroke [4]. This particular DOF is chosen to demonstrate the feasibility of our control implementation on the portion of the RiceWrist comprising the closed kinematic chain.

A. Experiment I: Validation of the Adaptive Controller

We first aimed at assessing whether the modified adaptive controller presented in Section III-A is able to estimate end-effector interaction forces F_p. In particular, we sought to determine if the implemented performance-dependent modification change in feedback gains affects the quality and accuracy of force estimation.

In *Experiment I*, we used a linear extension spring connected on one side to the robot handle, with the other side of the spring attached to a fixed frame. This setup was meant to provide a reproducible model of an impaired subject with stiff tendons. The spring is connected so that it is at its equilibrium point when the robot is approximately at its neutral configuration, and resists movement only in the wrist flexion region (positive FE), while it is not engaged for extension movements. The spring provides an approximate rotational stiffness, in robot end-effector coordinates, of 1.302 N · m/rad.

For the first part of the experiment, Experiment I-a, a sinusoidal desired trajectory with 22° amplitude and 0.5 Hz frequency is assigned for FE rotation while other joints are kept in a neutral pose (see Fig. 2). The adaptation gain Γ^{-1} ($\mathbf{diag}(0.0025\ 0.0025\ 0.0025\ 0.0025)$N · m/rad), Λ ($\mathbf{diag}(60\ 6\ 50\ 20)\frac{1}{\rm s}$), and K_D ($\mathbf{diag}(10\ 2.5\ 1.5\ 1.5)$N · ms/rad) are chosen experimentally such that the average steady state position error is less than 0.45° and the estimation of the feedforward part converges in approximately 140 s.

Fig. 7(a) shows the position error values for the first and last 10 s of *Experiment I-a*, and Fig. 7(b) shows the feedforward and feedback part of the control input in task space. The increase of the feedforward part in the region in which the spring is maximally deformed indicates that the adaptive controller successfully estimates F_p.

In order to assess the quality of force estimation, we analyzed the estimated values of unknown parameters related to the Gaussian RBFs after the controller reached steady state. Since *Experiment I-a* involved only a rotation of the FE joint, with the other joints kept at 0°, we considered only the values of the five RBFs that are involved in this movement located at 0° for the RUD and PS joints, and at −20°, −10°, 0°, 10°, and 20° for the FE joint. Because the linear spring resists the movement in the positive direction, the estimated values for 0°, 10°, and 20° are expected to show a linearly increasing trend, while RBFs in the negative direction are unloaded by the spring and thus should estimate a negligible torque, determined mainly by unmodeled effects. Fig. 8(a) shows the converged values of the

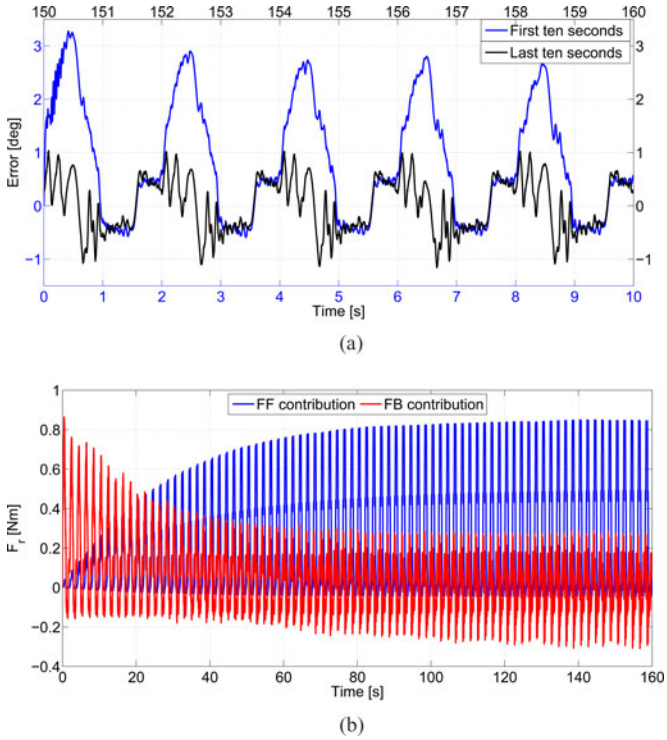

Fig. 7. *Experiment I-a*: Validation of the adaptive controller. (a) Errors for the first and last 10 s. Smaller error values can be achieved as the controller estimates the forces coming from the subject. (b) Feedforward and feedback components of the control input in task space. As the estimation progresses, the feedback decreases and feedforward dominates the response. Note that control input value is larger when the spring is resisting the movement.

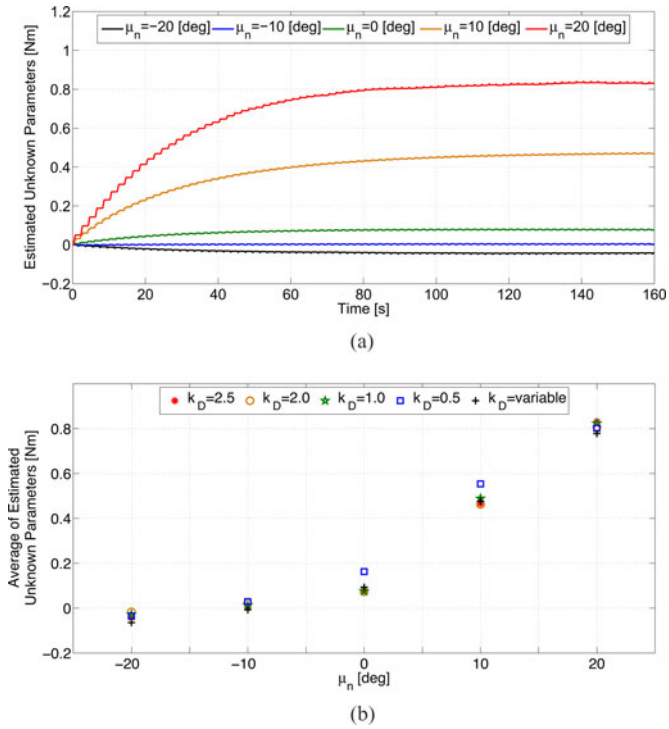

Fig. 8. *Experiment I-b*: Validation of the adaptive controller. (a) Converged values of Gaussian RBFs located at $\mu_n = -20°, -10°, 0°, 10°, 20°$ for the FE joint in *Experiment I-a*. (b) Estimated values for the last 20 s of *Experiment I-b* for different K_D values. The presented values are coherent with each other with a maximum deviation of 0.1 N·m that is caused mainly by modeling inaccuracies such as friction.

estimated Gaussian RBFs amplitudes, which agree well with the expected magnitudes.

Finally, we analyzed whether the implemented feedback gain modification algorithm compromises force field parameter estimation, compared to state-of-the-art constant feedback gain adaptive controllers. For this reason, in *Experiment I-b*, different K_D values are used for the control law, including the adaptive modification of the feedback gains described in (9). Fig. 8(b) presents the average of the estimated values for the last 20 s of *Experiment I-b* for different $k_{D,FE}$ values. The presented values are coherent with each other, as expected, with a maximum deviation of 0.1 N·m that is caused mainly by modeling inaccuracies such as friction.

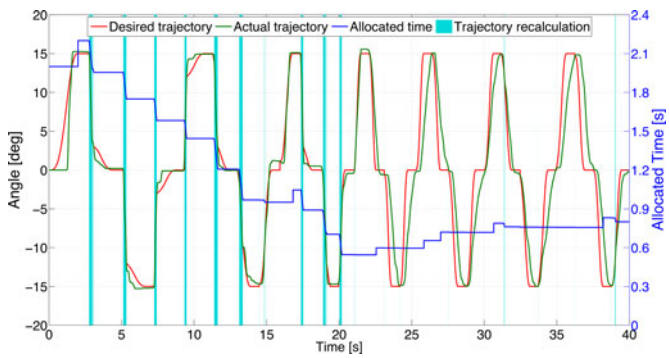

Fig. 9. *Experiment II*: Validation of real-time trajectory recalculation. The subject initially moves faster than the desired trajectory, causing several recalculations with corresponding decrease in total allocated time t_3. After a transient, the total time remains roughly constant at 0.8 s.

B. Experiment II: Validation of the Online Trajectory Recalculation Algorithm

Experiment II was conducted with one healthy subject in order to validate the real-time implementation of the described trajectory recalculation algorithm. The device was back-driven by the subject, who was asked to complete wrist pointing movements involving only wrist FE, with targets sequentially presented. The subject was instructed to reach the target as fast as he could. Therefore, t_3 was initially set to 2 s, ΔT was set to 0.002 s, and Δ was set to 1.1. The resulting pattern is shown in Fig. 9, showing that the trajectory recalculation algorithm is capable of reducing the allocated time when the subject is continuously overshooting the desired trajectory (i.e., in the early trials, $2.2 < t < 20$), and then increasing the time when the participant movements lag behind the nominal profile (i.e., after 20 s).

C. Experiment III: Validation of the AAN Controller Combined With the Online Trajectory Recalculation Algorithm

In *Experiment III*, the validation of the subject-adaptive controller, including both the AAN controller and the online

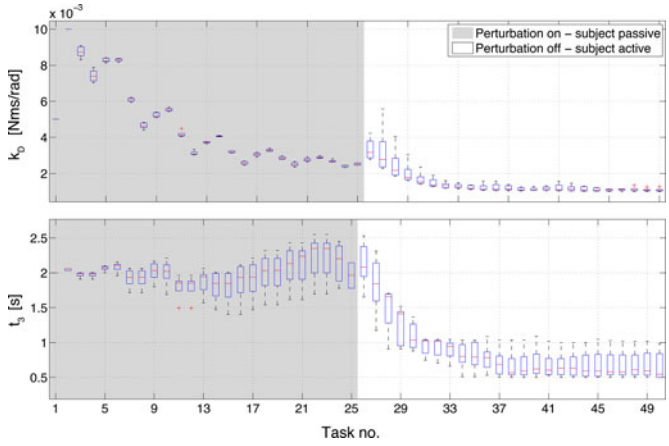

Fig. 10. *Experiment III*: Validation of the AAN controller combined with the online trajectory recalculation algorithm, for the experiment with five healthy subjects. (Top) Bar plot of the feedback gain value during each trial. (Bottom) Total allocated time for each trial (at the beginning of the trial). Gray-shaded area refers to the perturbation on, subject-passive phase. After 25 trials, the perturbation ceases and the subject is asked to complete the visually guided movements.

trajectory recalculation algorithm, was conducted with five healthy subjects, ages 23–30, interacting with the robot with their dominant arm. To explicitly test the capability of the controller to accommodate a subject whose force capabilities rapidly change during therapy, we structured the validation experiment in two phases. In the first phase, the subject was asked not to interfere with the robot, which was controlled through the algorithm described in the previous sections. During this phase, the robot applied a modified control action $F_{r,\mathrm{mod}} = F_r + c$, where F_r is the control input defined in (3), and c is a constant task space applied torque that mimics the action of a subject. After 60 s, c was instantaneously set to zero, and the subject was asked to move intentionally as triggered by the visual display.[2] The simulated instantaneous change of F_p represents an exaggerated scenario of a subject rapidly undergoing improvement of functional capabilities during therapy. We show that the subject-adaptive controller provides the desired characteristics for both modification of the feedback gain and update of the allocated time required to complete the trial.

During the perturbation on, subject-passive phase (shaded in gray in Fig. 10), the feedback modification algorithm first increases the assigned feedback gain, and as the adaptive controller estimates the constant task-space torque, decreases the gain until it settles down to a roughly constant value. During the perturbation off, subject active phase (not shaded in Fig. 10) $c = 0$, the subject is required to actively move. In this phase, k_D shows first-order decay dynamics, with update constant determined by parameter τ in (14). The maximum allocated time t_3 remains roughly constant during the perturbation on, subject passive condition, rapidly converging to a steady-state value within 10–15 trials after the transition to the subject-active condition (mean across all subjects 1.18 s, standard deviation in the last 12 trials 0.19 s). Higher variability in the dynamics of t_3 reflects different personal preferences in the accomplishment of the trial, whose "optimal" duration was not cued or controlled by any means. Approximately 10–15 trials after the entry in the subject active condition, however, t_3 did not significantly change within subjects (maximum standard deviation of t_3 in trials 15–25 in the subject active phase equals to 6% of the mean value).

[2]The following set of controller parameters was used: $k_{D,\mathrm{FE}}(1) = 5 \cdot 10^{-3}$ N·ms/rad, $k_{\mathrm{MIN,FE}} = 1 \cdot 10^{-3}$ N·ms/rad, $k_{\mathrm{MAX,FE}} = 2 \cdot 10^{-2}$ N·ms/rad, $r_{\mathrm{MIN,FE}}$ =0.5 rad/s, $r_{\mathrm{MAX,FE}}$ =15 rad/s, $\tau = 3$, c =0.2 N·m, $t_3(1,1) = 2$ s.

VI. Discussion and Conclusion

We have presented the development of a subject-adaptive controller that features an AAN controller with a feedback gain modification algorithm and a real-time trajectory generation algorithm. Together, these novel features enable the application of this controller to the RiceWrist robotic system, a therapeutic exoskeleton robot that has been developed to rehabilitate the distal DOF (forearm PS, wrist FE, and RUD) of the upper limb.

Previous AAN controllers for robotic rehabilitation have used impedance controllers to regulate assisting forces based on deviations from desired trajectories, but cannot adapt in the case of heterogeneous residual motor capabilities across the robot workspace. AAN controllers based on an adaptive control architecture offer this customization and are, therefore, selected for our application of wrist rehabilitation, since differential abilities to execute wrist FE movements are often observed in our target populations of stroke and incomplete spinal cord injury. To date, however, such adaptive AAN controllers have modified the feedforward part of the controller in order to adapt the estimate of the participant's ability to execute movements.

We introduce a novel AAN controller, designed to obtain ultimately bounded stability properties. Inspired by motor control studies showing that error is likely to be a driving signal for motor learning [9], [10], we developed a novel formulation based on feedback gain modification. Our formulation gives direct access to modify the allowable error during movement execution, while simultaneously estimating the forces provided by the participant that contribute to movement execution. Experimental results show that the controller accurately estimates environmental forces such as would be applied by the subject during therapy.

The approach presented in this paper translates the adaptive controller approach [19] to the field of rehabilitation robotics, and combines Gaussian RBFs for estimating interaction forces, as previously proposed in [16], and later proposed in [14] for rehabilitation applications. Our controller differs from [14] because we directly manipulate the admissible error bounds and the amount of force support. Hence, instead of requiring the errors to become zero, our controller tolerates error and manipulates the error bound in a performance-adaptive way. Furthermore, the proposed approach does not apply any modification to the adaptation law of the controller [19] and, therefore, does not interfere with the quality of force estimation.

The formulation is based on the working hypothesis that the subjects' applied force field (referred to as F_p in this paper)

is linearly parameterizable. Despite the simplifying nature of this assumption, the approach has been introduced in [18] for a real-time controller implementation, and in [17] for modeling of human motor control. Our experimental results show that the system is capable of rapidly adapting to the changing residual capabilities of subjects, even if the actual forces applied cannot be accurately modeled as a linearly parameterizable force field F_p. Although alternate methods of force estimation have the potential to provide more accurate estimation, they are model based, introduce complexity to the control algorithm, and increase computational cost. For example, the nonlinear disturbance observer proposed in [33] requires detailed modeling of the system, and the force estimation model proposed in a more recent study [34] requires both modeling of the system and measurement of the end-effector acceleration.

Because the RiceWrist is used to rehabilitate movements of the distal upper extremity, we must ensure that the desired trajectories are physiologically appropriate for wrist movements. Much of the prior literature in trajectory generation for upper limb rehabilitation robotics is based on the notion of optimally smooth (minimum jerk) movements. Such characteristics of upper limb movements have been reliably demonstrated for whole arm reaching tasks evaluated in task space. However, recent findings have indicated that the same characteristics are not observed in point-to-point reaching movements of the wrist joint. Therefore, we have presented results of an experiment with healthy subjects in order to define a physiological representation of a desired wrist movement profile that can be employed with our AAN controller. The resulting asymmetric single peak wrist pointing profiles are represented with beta functions, which facilitate online recalculation during movement execution. The online trajectory recalculation algorithm is presented and shown to be feasible for implementation with the RiceWrist.

Finally, the combination of the proposed AAN controller with feedback gain modification and online trajectory recalculation algorithm is validated through experiments involving five healthy subjects. Experimental results demonstrate that the proposed approach provides variable levels of mechanical assistance, when the subject is able to complete the movement on his own by estimating the forces provided by the subject, adapts the feedback gains so as to regulate the assistance in a performance-adaptive way, and updates the desired trajectory in real time based on the capabilities of the subject, as estimated via the AAN controller.

Future work will focus on the implementation of the RiceWrist with the modified adaptive AAN controller and online trajectory recalculation in a clinical setting, where we plan to validate the efficacy of our controller for rehabilitation of the distal upper limb after neurological injury, such as stroke or incomplete spinal cord injury.

APPENDIX

We follow the formulation presented in [21] to derive an accurate dynamical model of the parallel portion of the RiceWrist. The dynamic modeling approach is based on separating a generic parallel chain into a sub-set of rigid bodies or serial structures, described in terms of n' generalized coordinates q' ($n' > n$). After this operation, the system is actually composed of a *collection* of isolated dynamical systems (that can be either open chains with a known dynamical model or just isolated rigid bodies), each satisfying an equation of the form

$$M'(q')\ddot{q}' + C'(q', \dot{q}')\dot{q}' + g'(q)' = 0. \tag{26}$$

The goal of this approach is to find an analytical transformation between the matrices representing the model of the isolated system in (26) and the desired dynamical model expressed in (1). In order to do this, we need to express the $n' - n$ constraint equations, that for a holonomic system can be written in the form

$$\phi(q') = 0. \tag{27}$$

Equation (27) shows that the generalized coordinates q' are not in general independent, but are restricted to a subspace of $\Re^n$, namely to the domain $\mathbf{U}' = \{\mathbf{q}' \in \Re^{\mathbf{n}} : \phi(\mathbf{q}') = \mathbf{0}\}$ and are named *dependent generalized coordinates*.

Normally, it is possible to choose a set of n independent generalized coordinates x among the n' coordinates q'. In this case, the mapping between x and q' can be expressed by a selection function such that $x = \alpha(q')$. Combining this result with (27), the complete kinematic model of the parallel manipulator can be expressed as

$$\begin{bmatrix} \phi(q') \\ \alpha(q') \end{bmatrix} = \psi(q') = \begin{bmatrix} 0 \\ x \end{bmatrix}. \tag{28}$$

Accordingly, we can define the Jacobian matrix for to the generalized model as

$$\psi_{q'}(q') = \frac{\partial \psi}{\partial q'}. \tag{29}$$

When the manipulator is not in a singular configuration (i.e., $q' \in U' : \det[\psi_{q'}(q')] \neq 0$), the differential mapping between generalized and independent coordinates is expressed as

$$\dot{q}' = \rho(q')\dot{q} \tag{30}$$

where

$$\rho(q') = \psi_{q'}^{-1}(q') \begin{bmatrix} 0_{(n'-n)\times n} \\ I_{n\times n} \end{bmatrix}. \tag{31}$$

Under this formalism, it can be shown that a parallel system can be modeled in the form of (1), by calculating B, C, and g starting from the known functions B', C', and g' and imposing the kinematic constraint as

$$\begin{aligned} M(q') &= \rho(q')^T M'(q')\rho(q') \\ C(q, \dot{q}') &= \rho(q')^T C'(q', \dot{q}')\rho(q') + \rho(q')^T M'(q')\dot{\rho}(q', \dot{q}') \\ g(q') &= \rho(q')^T g'(q'). \end{aligned} \tag{32}$$

The use of the symbolic expressions shown in (32), in conjunction with the iterative solution of the forward kinematics problem to calculate the mapping $q' = \sigma(x)$, and with the differential mapping $\dot{q}' = \rho(q')\dot{x}$, allows simplification of the parallel dynamical modeling problem, into a simpler problem of modeling m disjoint serial kinematic chains.

The described method has been applied to the parallel portion of the RiceWrist. For this manipulator, (27) can be expressed in symbolic form, as a function of the generalized coordinates $q' = [\theta_1, \theta_2, \theta_3, \alpha, \beta, \gamma, X_C, Y_C, Z_C, l_l, l_2, l_3]^T$. The model can be converted in the end-effector frame defined by coordinates $x = [\alpha, \beta, Z_C]^T$ by 1) differentiation of the constraint equations, 2) separation of the parallel manipulator in a set of disjointed serial chains and rigid bodies with known dynamical models, and 3) application of (32).

Step 1 has been accomplished using symbolic calculation. Step 2 has been accomplished by splitting the manipulator at the level of the spherical joints, dividing the parallel manipulator in three 2-DOF serial revolute-prismatic (RP) manipulators and a rigid body, the platform $B_1B_2B_3$, which applies the interaction forces and torques with the subject. For the serial RP manipulator, the dynamical equations can be easily computed using the Lagrangian approach, as a function of the coordinates $q_i' = [\theta_i, l_1]^T$, thus obtaining

$$M_i' = \begin{bmatrix} m_i(l_i - l_0)^2 + I_i + I_{g,i} & 0 \\ 0 & m_i \end{bmatrix}$$
$$C_i' = \begin{bmatrix} m_i(l_i - l_0)\dot{l}_i & m_i(l_i - l_0)\dot{\theta}_i \\ -m_i(l_i - l_0)\dot{\theta}_i & 0 \end{bmatrix} \quad (33)$$
$$g_i' = \begin{bmatrix} m_i(l_i - l_0)g_i \cos\theta_i \\ m_i g_i \end{bmatrix}$$

where m_i refers to the mass of the sliders of the prismatic joint with length l_i, $I_{g,i}$ to the sliders' baricentral moment of inertia, I_i to the movement of inertia of the rotating part supporting the sliders (which will later be neglected), g_i is the component of the gravity vector projected along the slider's axis, and l_0 is the half length of the sliders. Concatenating the matrices defined above for the three serial manipulators, and employing cardinal equations of dynamics for the platform, yields the matrices M', C', and the vector function g', needed for (32). Parameters reported in (33) have been measured from CAD drawings of machined parts, and the subject hand has been modeled as a pure inertia, with a mass of 1 kg, providing an overly conservative estimate of torques obtained through inverse dynamics in Section II.

REFERENCES

[1] A. Go, D. Mozaffarian, V. Roger, E. Benjamin, J. Berry, W. Borden, D. Bravata, S. Dai, E. Ford, C. Fox, S. Franco, H. Fullerton, C. Gillespie, S. Hailpern, J. Heit, V. Howard, M. Huffman, B. Kissela, S. Kittner, D. Lackland, J. Lichtman, L. Lisabeth, D. Magid, G. Marcus, A. Marelli, D. Matchar, D. McGuine, E. Mohler, C. Moy, M. Mussolino, G. Nichol, N. Paynter, P. Schreiner, P. Sorlie, J. Stein, T. Turan, S. Virani, N. Wong, D. Woo, and M. Turner, "Heart disease and stroke statistics—2013 update: A report from the American Heart Association," *Circulation*, vol. 127, pp. e6–e245, 2013.

[2] National Spinal Cord Injury Statistical Center Report, "Spinal cord injury facts and figures at a glance," *J. Spinal Cord Med.*, vol. 36, no. 2, pp. 170–171, 2013.

[3] M. Berkowitz, *Spinal Cord Injury: An Analysis of Medical and Social Costs*. New York, NY, USA: Demos Medical Publishing, 1998.

[4] C. Bütefisch, H. Hummelsheim, P. Denzler, and K. Mauritz, "Repetitive training of isolated movements improves the outcome of motor rehabilitation of the centrally paretic hand," *J. Neurol. Sci.*, vol. 130, no. 1, pp. 59–68, 1995.

[5] A. Lo, P. Guarino, L. Richards, J. Haselkorn, G. Wittenberg, D. Federman, R. Ringer, T. Wagner, H. Krebs, B. Volpe, C. Bever Jr., D. Bravata, P. Duncan, B. Corn, A. Maffucci, S. Nadeau, S. Conroy, J. Powell, G. Huang, and P. Peduzzi, "Robot-assisted therapy for long-term upper-limb impairment after stroke," *N. Engl. J. Med.*, vol. 362, no. 19, pp. 1772–1783, 2010.

[6] N. Yozbatiran, J. Berliner, M. K. O'Malley, A. U. Pehlivan, Z. Kadivar, C. Boake, and G. E. Francisco, "Robotic training and clinical assessment of upper extremity movements after spinal cord injury: A single case report," *J. Rehabil. Med.*, vol. 44, no. 2, pp. 186–188, 2012.

[7] L. Marchal-Crespo and D. Reinkensmeyer, "Review of control strategies for robotic movement training after neurologic injury," *J. Neuroeng. Rehabil.*, vol. 6, no. 1, pp. 1–15, 2009.

[8] N. Hogan, H. Krebs, B. Rohrer, J. Palazzolo, L. Dipietro, S. Fasoli, J. Stein, R. Hughes, W. Frontera, D. Lynch, and B. Volpe, "Motions or muscles? Some behavioral factors underlying robotic assistance of motor recovery," *J. Rehabil. Res. Develop.*, vol. 43, no. 5, p. 605, 2006.

[9] J. L. McClelland, D. E. Rumelhart, and P. R. Group, *Parallel Distributed Processing: Explorations in the Microstructure of Cognition*, vol. 2. Cambridge, MA, USA: MIT Press, 1986.

[10] S. G. Lisberger, "The neural basis for learning of simple motor skills," *Science*, vol. 242, no. 4879, pp. 728–735, 1988.

[11] H. I. Krebs, J. J. Palazzolo, L. Dipietro, M. Ferraro, J. Krol, K. Rannekleiv, B. T. Volpe, and N. Hogan, "Rehabilitation robotics: Performance-based progressive robot-assisted therapy," *Auton. Robots*, vol. 15, no. 1, pp. 7–20, 2003.

[12] Y. Mao and S. K. Agrawal, "Design of a cable-driven arm exoskeleton (CAREX) for neural rehabilitation," *IEEE Trans. Robot.*, vol. 28, no. 4, pp. 922–931, Aug. 2012.

[13] V. Squeri, L. Masia, P. Giannoni, G. Sandini, and P. Morasso, "Wrist rehabilitation in chronic stroke patients by means of adaptive, progressive robot aided therapy," *IEEE Trans. Neural Syst. Rehabil. Eng.*, vol. 22, no. 2, pp. 312–325, Mar. 2014.

[14] E. Wolbrecht, V. Chan, D. Reinkensmeyer, and J. Bobrow, "Optimizing compliant, model-based robotic assistance to promote neurorehabilitation," *IEEE Trans. Neural Syst. Rehabil.*, vol. 16, no. 3, pp. 286–297, Jun. 2008.

[15] R. Sanchez Jr, E. Wolbrecht, R. Smith, J. Liu, S. Rao, S. Cramer, T. Rahman, J. Bobrow, and D. Reinkensmeyer, "A pneumatic robot for re-training arm movement after stroke: Rationale and mechanical design," in *Proc. IEEE 9th Int. Conf. Rehabil. Robot.*, 2005, pp. 500–504.

[16] R. M. Sanner and J.-J. Slotine, "Gaussian networks for direct adaptive control," *IEEE Trans. Neural Netw.*, vol. 3, no. 6, pp. 837–863, Nov. 1992.

[17] R. M. Sanner and M. Kosha, "A mathematical model of the adaptive control of human arm motions," *Biol. Cybern.*, vol. 80, no. 5, pp. 369–382, 1999.

[18] E. Wolbrecht, "Adaptive, assist-as-needed control of a pneumatic orthosis for optimizing robotic movement therapy following stroke," *Ph.D. dissertation, Dept. Mech. Aerosp. Eng., Univ.* California, Irvine, CA, USA, 2007.

[19] J. Slotine and W. Li, "On the adaptive control of robot manipulators," *Int. J. Robot. Res.*, vol. 6, no. 3, pp. 49–59, 1987.

[20] A. Gupta, M. K. O'Malley, V. Patoglu, and C. Burgar, "Design, control and performance of RiceWrist: A force feedback wrist exoskeleton for rehabilitation and training," *Int. J. Robot. Res.*, vol. 27, no. 2, pp. 233–251, 2008.

[21] F. H. Ghorbel, O. Chételat, R. Gunawardana, and R. Longchamp, "Modeling and set point control of closed-chain mechanisms: Theory and experiment," *IEEE Trans. Control Syst. Technol.*, vol. 8, no. 5, pp. 801–815, Sep. 2000.

[22] A. U. Pehlivan, F. Sergi, and M. K. OMalley, "Adaptive control of a serial-in-parallel robotic rehabilitation device," in *Proc. IEEE Int. Conf. Rehabil. Robot.*, 2013, pp. 1–6.

[23] F. Girosi and T. Poggio, "Networks and the best approximation property," *Biol. Cybern.*, vol. 63, no. 3, pp. 169–176, 1990.

[24] R. Shadmehr, F. A. Mussa-Ivaldi, and E. Bizzi, "Postural force fields of the human arm and their role in generating multijoint movements," *J. Neurosci.*, vol. 13, no. 1, pp. 45–62, 1993.

[25] S. K. Charles and N. Hogan, "Stiffness, not inertial coupling, determines path curvature of wrist motions," *J. Neurophysiol.*, vol. 107, no. 4, pp. 1230–1240, Feb. 2012.

[26] D. Formica, S. K. Charles, L. Zollo, E. Guglielmelli, N. Hogan, and H. I. Krebs, "The Passive stiffness of the wrist and forearm," *J. Neurophysiol.*, vol. 108, no. 4, pp. 1158–1166, Aug. 2012.

[27] L. Vaisman, L. Dipietro, and H. I. Krebs, "A comparative analysis of speed profile models for wrist pointing movements," *IEEE Trans. Neural Syst. Rehabil. Eng.*, vol. 21, no. 5, pp. 756–766, Dec. 2013.
[28] C. M. Jarque and A. K. Bera, "A Test for Normality of Observations and Regression Residuals," *Int. Stat. Rev.*, vol. 55, pp. 163–172, May. 1987.
[29] F. Wilcoxon, "Individual Comparisons by Ranking Methods," *Biometrics Bull.*, vol. 1, no. 6, pp. 80–83, 1945.
[30] J. D. Gibbons and S. Chakraborti, "One-sample and paired-sample procedures," in *Nonparametric Statistical Inference*, 4th ed. Boca Raton, FL, USA: CRC Press, 2003.
[31] R. Plamondon, A. M. Alimi, P. Yergeau, and F. Leclerc, "Modelling velocity profiles of rapid movements: A comparative study," *Biol. Cybern.*, vol. 69, no. 2, pp. 119–128, 1993.
[32] H. I. Krebs, M. L. Aisen, B. T. Volpe, and N. Hogan, "Quantization of continuous arm movements in humans with brain injury," *Proc. Nat. Acad. Sci. USA*, vol. 96, pp. 4645–4649, Apr. 1999.
[33] A. Gupta and M. K. OMalley, "Disturbance-observer-based force estimation for haptic feedback," *J. Dyn. Syst. Meas. Control*, vol. 133, no. 1, pp. 014505-1–014505-4, 2011.
[34] M. Dyck and M. Tavakoli, "Measuring the dynamic impedance of the human arm without a force sensor" in *Proc. IEEE Int. Conf. Rehabil. Robot.*, 2013, pp. 1–8.

Ali Utku Pehlivan (S'11) received the B.S. degree in mechatronics engineering from Sabanci University Istanbul, Istanbul, Turkey, in 2009, and the M.S. degree in mechanical engineering from Rice University, Houston, TX, USA, in 2012. He is currently working toward the Ph.D. degree at the Mechanical Engineering Department, Rice University as a Member of Mechatronics and Haptic Interfaces Laboratory.

His research interests include exoskeletal robotic device design, nonlinear control, robotic rehabilitation, mechatronics, and robotics.

Fabrizio Sergi (M'12) received the M.S. and Ph.D. degrees in biomedical engineering from Università Campus Bio-Medico di Roma, Rome, Italy, in 2007 and 2011, respectively.

He is currently a Research Scientist in the Department of Mechanical Engineering, Rice University, Houston, TX, USA. His current research interests include wearable robotics, robot-aided neurorehabilitation, and human motor control.

Marcia K. O'Malley (SM'13) received the B.S. degree in mechanical engineering from Purdue University, West Lafayette, IN, USA, in 1996, and the M.S. and Ph.D. degrees in mechanical engineering from Vanderbilt University, Nashville, TN, USA, in 1999 and 2001, respectively.

She is currently an Associate Professor of mechanical engineering and computer science, Rice University, Houston, TX, USA, and directs the Mechatronics and Haptic Interfaces Laboratory. She is an Adjunct Associate Professor in the Departments of Physical Medicine and Rehabilitation in both Baylor College of Medicine and the University of Texas Medical School at Houston. Also, she is the Director of Rehabilitation Engineering at TIRR-Memorial Hermann Hospital, and is a cofounder of Houston Medical Robotics, Inc. Her research addresses issues that arise when humans physically interact with robotic systems, with a focus on training and rehabilitation in virtual environments.

Dr. O'Malley received the George R. Brown Award for Superior Teaching at Rice University in 2008. She is a 2004 Office of Naval Research Young Investigator and received the National Science Foundation Career Award in 2005. She is a Fellow of the American Society of Mechanical Engineers.